Molecular Neurobiology (2019) 56:1972–1983
https://doi.org/10.1007/s12035-018-1197-3

Small Molecule GSK-J1 Affects Differentiation of Specific Neuronal Subtypes in Developing Rat Retina

Reza Raeisossadati[1] · Marília Inês Móvio[1] · Lais Takata Walter[1] · Silvia Honda Takada[1] · Carolina Beltrame Del Debbio[2] · Alexandre Hiroaki Kihara[1,3]

Received: 21 February 2018 / Accepted: 26 June 2018 / Published online: 7 July 2018

Abstract

Histone post-translational modification has been shown to play a pivotal role in regulating gene expression and fate determination during the development of the central nervous system. Application of pharmacological blockers that control histone methylation status has been considered a promising avenue to control abnormal developmental processes and diseases as well. In this study, we focused on the role of potent histone demethylase inhibitor GSK-J1 as a blocker of Jumonji domain-containing protein 3 (Jmjd3) in early postnatal retinal development. Jmjd3 participates in different processes such as cell proliferation, apoptosis, differentiation, senescence, and cell reprogramming via demethylation of histone 3 lysine 27 trimethylation status (H3K27 me3). As a first approach, we determined the localization of Jmjd3 in neonate and adult rat retina. We observed that Jmjd3 accumulation is higher in the adult retina, which is consistent with the localization in the differentiated neurons, including ganglion cells in the retina of neonate rats. At this developmental age, we also observed the presence of Jmjd3 in undifferentiated cells. Also, we confirmed that GSK-J1 caused the increase in the H3k27 me3 levels in the retinas of neonate rats. We next examined the functional consequences of GSK-J1 treatment on retinal development. Interestingly, injection of GSK-J1 simultaneously increased the number of proliferative and apoptotic cells. Furthermore, an increased number of immature cells were detected in the outer plexiform layer, with longer neuronal processes. Finally, the influence of GSK-J1 on postnatal retinal cytogenesis was examined. Interestingly, GSK-J1 specifically caused a significant decrease in the number of PKCα-positive cells, which is a reliable marker of rod-on bipolar cells, showing no significant effects on the differentiation of other retinal subtypes. To our knowledge, these data provide the first evidence that in vivo pharmacological blocking of histone demethylase by GSK-J1 affects differentiation of specific neuronal subtypes. In summary, our results indisputably revealed that the application of GSK-J1 could influence cell proliferation, maturation, apoptosis induction, and specific cell determination. With this, we were able to provide evidence that this small molecule can be explored in therapeutic strategies for the abnormal development and diseases of the central nervous system.

Keywords Histone modification · Jmjd3 · Retinal development · Cell specification · Cell commitment · Epigenetics

Introduction

The mammalian central nervous system (CNS) is extremely complex in both architecture and function. During the formation of CNS, a variety of morphologically and functionally distinct cell types are generated from common proliferative cells. In retinal development, retinal progenitor cells (RPCs) undergo differentiation in a meticulous spatiotemporal order to generate different cell types [1]. Subsequent cellular differentiation depends on the synchronized and combinatorial influences of gene expression, which are regulated by sets of transcription factors [2]. Recently, it has been evidenced that epigenetic mechanisms can serve as gatekeepers for the activity of transcription factors [3]. Increasing evidence has shed light on the importance of many epigenetic regulation paths in retinal cell fate determination and maintenance [4, 5].

In recent years, molecular machinery of post-translational modifications of histones has been investigated [6–8]. Methylation of histone 3 lysine 27 residues

✉ Alexandre Hiroaki Kihara
alexandrekihara@gmail.com

[1] Laboratório de Neurogenética, Centro de Matemática, Computação e Cognição, Universidade Federal do ABC, R. Arcturus 3, Jardim Antares, São Bernardo do Campo, SP 09606-070, Brazil

[2] Departamento de Biologia Celular e do Desenvolvimento, Instituto de Ciências Biomédicas, Universidade de São Paulo, São Paulo, Brazil

[3] Departamento de Fisiologia e Biofísica, Instituto de Ciências Biomédicas, Universidade de São Paulo, São Paulo, Brazil

(H3k27 me2/3) is one of the key repressive modifications, which is mediated by polycomb repressive complex 2, with the enzymatic activity of histone methyltransferase enhancer of the zeste homolog 2 (Ezh2) [9–11], which has important roles in the retinal cell fate determination [12–14]. On the other hand, H3K27 demethylases such as Jumonji domain-containing protein 3 (Jmjd3), histone demethylase 6A (Utx), and ubiquitously transcribed tetratricopeptide repeat containing, Y-linked (Uty) contain highly homologous JmjC domains which are responsible for removing the methyl group from lysine 27 residue [15]. Specifically, Jmjd3 has several roles in the developmental process. For example, it activates the adult neurogenesis in the subventricular zone (SVZ), is necessary for bipolar cell differentiation [16–18], and is involved in neural lineage commitment [17]. Besides loss and gain of function studies with different genetic tools, small molecule inhibitors targeting different histone modifications have been applied in developmental biology and cancer investigation to develop epigenetic drugs for therapeutic intervention [19].

In this study, we uncovered the effects of GSK-J1 as a blocker of Jmjd3 in developing retina. We were able to determine the association of Jmjd3 with H3k27 trimethylation status (H3k27 me3) and the consequences on distinct aspects of development, such as cell cycle maintenance, proliferation, apoptosis induction, and differentiation of specific neuronal subtypes. We provide evidence that GSK-J1 can be explored in therapeutic strategies aimed for the treatment of abnormal development and diseases of the CNS.

Materials and Methods

Ethics Statement and Animals

All experiments were performed in Long Evans rats (*Rattus norvegicus*). The experiments on animals were conducted considering the guidelines of the NIH and the Brazilian Society for Laboratory Animals. The experimental protocol (9965240217) was approved by the Ethics Committee of Federal University of ABC. All injections were performed under anesthesia, and all efforts were made to minimize the suffering. Long Evans rat pups were housed in home cages at the vivarium of University Federal ABC under 12:12 h light/dark cycle and at a constant temperature (23 ± 1 °C).

Subretinal Injection

Neonate (P0) rat pups were anesthetized by isoflurane gas inhalation, and the eyelid was cut. The eyelids were pulled apart with curved forceps to expose the eyeball for injection. Two microliters of vehicle or blocker were injected in the subretinal space using pulled glass needle attached to a 10-μL Hamilton syringe (7635-01, Hamilton syringes, Hamilton Company, Reno, NV, USA) as previously described in experiments carried out in developing mice [20] and rats [20]. In each animal, one eye was used as control (5% dimethyl sulfoxide [DMSO] diluted in phosphate-buffered saline [PBS]), and the other eye was injected with the blocker (GSK-J1 [SML0709, Sigma, St. Louis, Missouri, USA] 1 mM, diluted in 5% DMSO + PBS). After each injection, the overall morphology of the eye and the integrity of the retina were evaluated.

Immunofluorescence Experiments

The retinas were dissected and fixed for 4 h in 4% paraformaldehyde (PFA) in phosphate buffer 0.1 M (PB) at pH 7.3 and cryoprotected in 30% sucrose solution for at least 24 h at 4 °C. Following the embedding in O.C.T. compound (25608-930, Sakura Finetek, Torrance, CA, USA), the samples were cut transversally (12 μm) on a cryostat. As previously described, for whole mount experiments, the retinas were fixed in 4% PFA in PB for 24 h at 4 °C before incubation with the primary antibody [21]. The sections or whole mounts were incubated overnight or 7 days, respectively, with the primary antibodies in a solution containing 5% normal donkey serum or 5% normal goat serum and 0.5% Triton-X 100 in 0.1 M PBS at room temperature; the antibodies and concentrations are listed in Table 1. After several washes, the sections were incubated for 2 h and the whole mounts for 24 h with donkey/goat antiserum against rabbit, mouse, or goat IgG tagged to Alexa 488 (1:250–1:500, Invitrogen, Carlsbad, CA, USA) at room temperature. 4,6-Diamidino-2-phenylindole (DAPI) was diluted in the same incubation solution of the secondary antibodies to counterstain the retinal sections. Controls for the experiments consisted of the omission of primary antibodies; no staining was observed in these cases. After washing, the tissue was mounted using Vecta Shield (H-1000, Vector Labs, Burlingame, CA, USA).

Table 1 List of antibodies and respective concentrations

Antibody	Manufacturer	Product number	Dilution
Ki67	Bd Bioscience	556,003	1:100
KDM6B/Jmjd3	Abcam	ab169197	1:200
Parvalbumin	Thermo Fisher	PA1-933	1:200
ChAT	Millipore	AB144P	1:100
Brn3a	Santa Cruz	sc-8429	1:100
PKCα	Sigma	P5704	1:100
DCX	Abcam	ab18723	1:200
BrdU	Life Technologies	B3512B	1:200
H3k27me3	Abcam	ab6002	1:5000
H3	Abcam	ab1791	1:5000

TUNEL Assay

Click-iT® Plus TUNEL Assay (C10617, Life Technologies, OR, USA) was utilized for the TUNEL staining, according to the manufacturer's protocol. All figures were captured using a fluorescence microscope (DM 5500, Leica Microsystems, Wetzlar, Germany). The figures were mounted with Adobe Photoshop CS. The manipulation of the images was restricted to brightness and contrast adjustments of the whole image.

Histone Isolation and Immunoblotting

The retinas were dissected ($N = 6$, each group) 24 h following the subretinal injections, and histones were isolated using a histone extraction kit (ab113476, Abcam, Cambridge, UK). The histone concentration was determined by the BCA method (#23225, Thermo Scientific, Rockford, IL, USA), according to the manufacturer's protocol. For western blots, the proteins (2 μg) were separated by 13.5% SDS-PAGE and transferred to nitrocellulose membranes. The membranes were blocked with 5% non-fat milk in Tris-buffered saline with Tween 20 (TBST) buffer for 90 min at room temperature, subsequently rinsed in TBST and incubated with antibodies against H3k27 me3 (ab6002, Abcam) overnight at 4 °C; then, the membranes were rinsed in TBST and incubated with mouse conjugated to horseradish peroxidase (HRP) enzyme (1 : 5000, Invitrogen, Carlsbad, CA, USA) for 2 h at room temperature. The detection of the labeled proteins was achieved by using the enhanced chemiluminescent system (RPN2132, ECL kit; GE Healthcare, Little Chalfont, UK). For normalization, the membranes were stripped, rinsed, re-blocked, and probed with anti-H3 (ab1791, Abcam), followed by incubation with an antibody raised against mouse conjugated to HRP enzyme (1:5000, Invitrogen). Optical density measurement was performed by ImageJ software (National Institute of Mental Health, Bethesda, Maryland, USA). The paired two-tailed *t* test was applied for statistical analysis.

BrdU Labeling

5-Bromo-2′-deoxyuridine (BrdU) (B5002, Sigma) 100 mg/kg body weight was injected intraperitoneally (IP) in P0 pups to label the S-phase proliferative cells. Following the IP injection, the subretinal injection was performed. After 48 h, the retinas were dissected and processed for anti-BrdU staining with the addition of a pre-treatment step with 2N HCl for 30 min at 37 °C.

Image Quantification and Statistical Analysis

During retinal development, differences in several parameters can be observed depending on the eccentricity, including cellular proliferation, apoptosis, differentiation, and maturation. In our study, the values used for statistical analysis were obtained for the central retina. The *n* described in each experiment reflects the number of animals from which we obtained eight to ten sections per retina (12 mm thickness). After quantifying in the sections, we used the median value for each animal. For each section, at least six images were used, with × 40 magnification for microtubule-associated protein

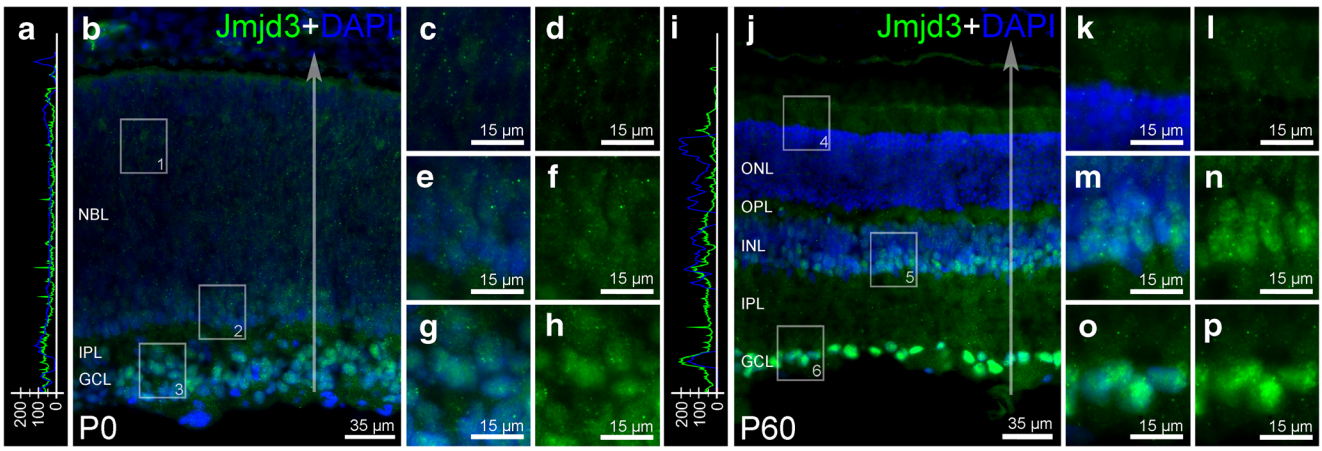

Fig. 1 Immunofluorescence analysis of Jumonji domain-containing protein 3 (Jmjd3, green) in transverse sections of developing and adult rat retina counterstained with 4′,6-diamidino-2-phenylindole (DAPI, blue). **a**, **b** Pixel analysis and representative immunostaining of Jmjd3 in the neonate (P0) rat retinal section. **c**, **d** High magnification of selected area 1 showing Jmjd3 labeling in the outer part of the neuroblastic layer (NBL). **e**, **f** High magnification of selected area 2 showing the accumulation of Jmjd3 in the inner part of NBL. **g**, **h** High magnification of selected area 3 showing nuclear accumulation of Jmjd3 in cells located in the ganglion cell layer (GCL). **i**, **j** Pixel analysis and representative immunostaining of Jmjd3 in adult (P60) rat retinal section. **k**, **l** High magnification of selected area 4 showing Jmjd3 labeling in presumptive inner segments of photoreceptors and cytoplasm of cells located in the outer nuclear layer (ONL). **m**, **n** High magnification of selected area 5 showing Jmjd3 labeling in cells located in the inner part of the inner nuclear layer (INL). **o**, **p** High magnification of selected area 6 showing Jmjd3 labeling in cells located in the GCL

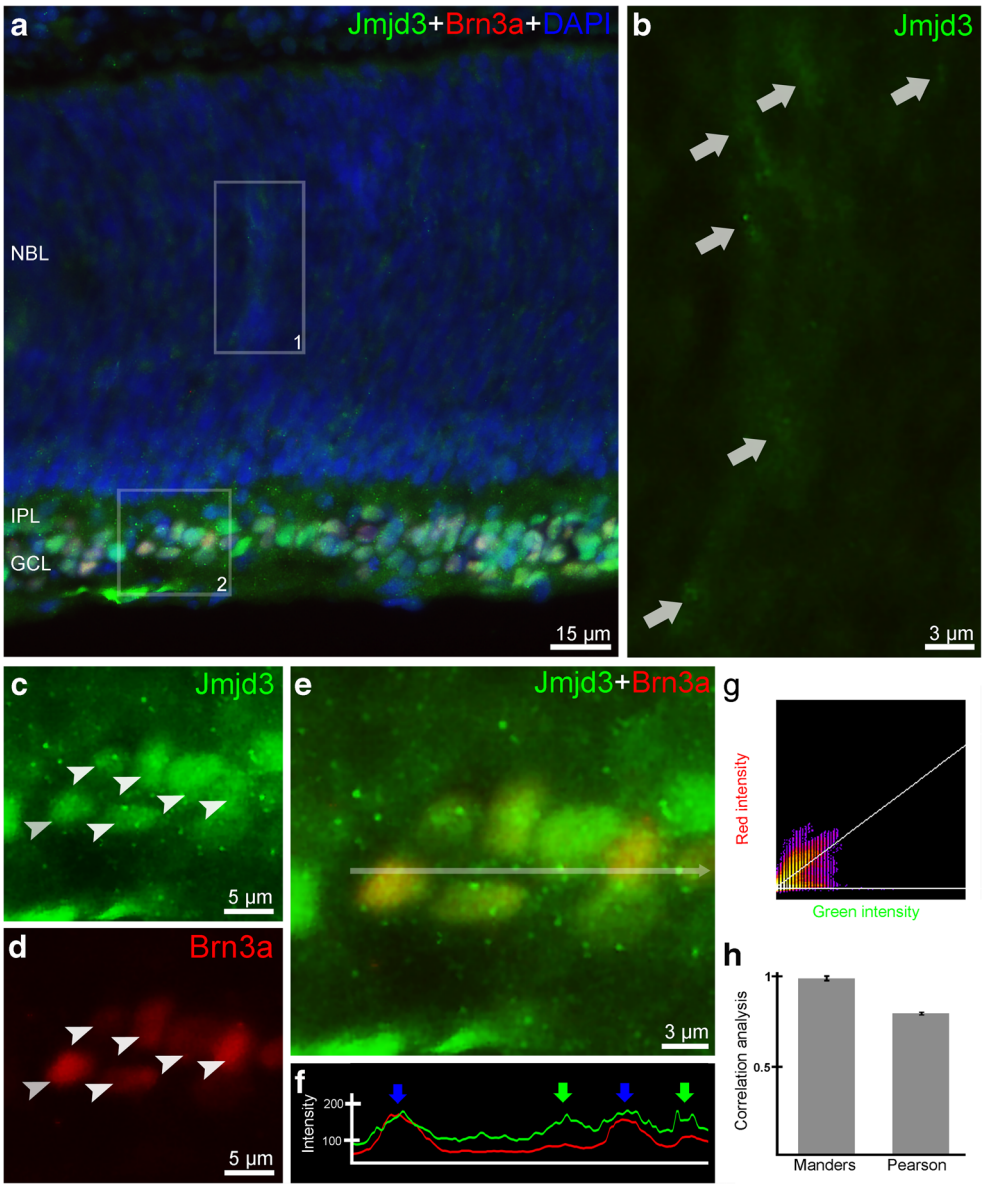

Fig. 2 Immunofluorescence and colocalization analysis of Jumonji domain-containing 3 (Jmjd3, green) and brain-specific homeobox/POU domain protein 3A (Brn3a, red) in transverse sections of developing rat retina counterstained with 4′,6-diamidino-2-phenylindole (DAPI, blue). **a** Representative double-labeling image using anti-Jmjd3 and ganglion cell marker anti-Brn3a in the neonate (P0) rat retina. **b** High magnification of selected area 1 with the arrows indicating weak immunofluorescence signal in the neuroblastic layer (NBL). **c**–**e** High magnification of selected area 2 with the arrowheads indicating accumulation of Jmjd3 in ganglion cell layer (GCL). The same Jmjd3-positive cells located in GCL are also stained with anti-Brn3a. **f** Pixel intensity analysis indicating that in spite of the ubiquitous immunolabeling of Jmjd3 in GCL (green arrows), the overlap of green and red signals is visible (blue arrows). **g** Color-coded scattergram represents the correlation between the intensity of the green and red channels. **h** Manders' and Pearson's correlation analyses were also performed in these experiments, revealing both high spatial coincidence and intensity correlation between red and green channels

doublecortin (DCX) immunolabeling and × 20 magnification for other purposes, with the fluorescence microscope (DM 5500, Leica Microsystems). Image analyses were performed with ImageJ software using several plug-ins (National Institute of Mental Health, Bethesda, MD, USA) as previously described [21]. The numbers and the length of the filaments for DCX were measured by neuronJ plug-in. BrdU-positive cells were counted with MBF plug-in and manually checked. The TUNEL-positive cells were counted with TUNEL cell counter plug-in. The colocalization was performed with Coloc 2 plug-in. This plug-in initially generates an 8-bits image with only the colocalized points; then, it combines the three 8-bits images into an RGB image. Two points are considered as colocalized if their respective intensities are strictly higher than the threshold of their channels, which is 50 by default, and if their ratio of intensity is strictly higher than the ratio setting value, which is 50%. This plug-in also provided values obtained in Manders' and Pearson's correlation. Manders' colocalization coefficients (MCC) are widely used to analyze fluorescent images. For two probes, denoted as R and G, two different MCC values are derived, M_1, the fraction of R in compartments containing G, and M_2, the fraction of G in compartments containing R. In turn, Pearson's correlation coefficient values range from one for two images whose fluorescence intensities are perfectly, linearly related to − 1 for two images whose fluorescence intensities are perfectly, but inversely, related to one another. Values near zero reflect distributions of probes that are uncorrelated with one another [22]. Pixel profiles were made by Nikon TS100F (Nikon Instruments Inc., Melville, NY, USA.). The number of Ki67- and PKC-positive cells was counted manually using the Cell Counter plug-in of ImageJ. The paired two-tailed t test was

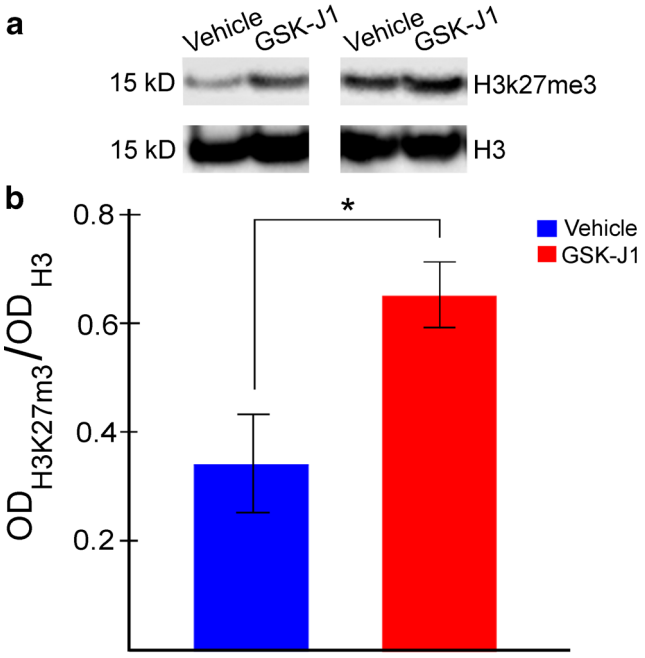

Fig. 3 Regulation of histone 3 lysine 27 trimethylation status (H3k27 me3) in developing rat retina after GSK-J1 subretinal injection. **a** Representative bands obtained using anti-H3k27 me3 and anti-histone 3 (H3) internal control 24 h after subretinal injection of vehicle and GSK-J1. **b** Quantification of the bands revealed changes in H3k27 me3 levels on comparing controls (blue) with GSK-J1-treated retinas (red) ($P = 0.0494$, $n = 6$ per group)

applied for all statistical analysis with Excel (Microsoft, Redmond, WA, USA). All the data were recorded as mean of differences and standard error of the mean. The images and charts were prepared using Adobe Photoshop CC 2014 (Adobe Systems Inc., San Jose, CA, USA).

Results

Jmjd3 Spatial Localization Changes in Developing and Adult Retina

We first examined the distribution pattern of Jmjd3 in P0 and adult (P60) rat retinas. We observed that Jmjd3 labeling accumulated mainly in the cell nuclei in both ages. In P0 retinas, Jmjd3 was localized in the ganglion cell layer (GCL) and also in neuroblastic layer (NBL) (Fig. 1a–h). In P60 retinas, Jmjd3 labeling was observed in the GCL and also in the inner nuclear layer (INL) (Fig. 1i–p).

Double-labeling with Brn3a, a marker of ganglion cells, was performed in P0 rat retinas to confirm that Jmjd3 accumulates in differentiated ganglion cells. The colocalization seen in the immunostaining images was supported by high values obtained in Manders' (0.98 ± 0.02) and Pearson's (0.80 ± 0.01) correlation analyses, confirming that Jmjd3 accumulates in ganglion cells located in the GCL (Fig. 2).

GSK-J1 Enhances H3k27 me3 Levels in Developing Retina

Since Jmjd3 might affect H3K27 me3 methylation, we measured the levels of H3K27 me3 by western blotting after GSK-J1 treatment. The global change in the H3K27 me3 levels was determined by quantitative western blotting in which we calculated the ratio of H3K27 me3 normalized by total H3 in vehicle-injected versus blocker-injected eyes after 24 h ($n = 6$ per group). We were able to determine that the normalized level of H3K27 me3 is significantly higher (0.32 ± 0.11 vs. 0.64 ± 0.07, $P = 0.0494$) in the blocker-treated retinas (Fig. 3). As expected, we were not able to detect changes in the H3 protein levels (8431 ± 297 vs. 7749 ± 251, $P = 0.3076$).

GSK-J1 Enhances the Accumulation of Cell Cycle Marker Ki67 and Cell Proliferation in Developing Retina

To address the impact of the Jmjd3 blockade on cell cycle, we evaluated Ki67 accumulation in P2 retinal cells after subretinal injection of GSK-J1 in P0 rats (Fig. 4). We were able to determine that the number of Ki67-positive cells in the outer NBL increased significantly after the blockade of Jmjd3 (2.71 ± 0.01 vs. 3.78 ± 0.24, $P = 0.0348$).

Subsequently, BrdU intraperitoneal injection was performed following the subretinal injection in P0 pups ($n = 6$ per group). We demonstrated that when compared with the controls, the number of BrdU-positive cells in the retina increased significantly in the GSK-J1-injected eyes after 48 h (11.81 ± 0.56 vs. 15.03 ± 0.77, $P = 0.0116$; Fig. 5c). The number of positively stained cells in the GCL did not significantly change (2.84 ± 0.59 vs. 3.79 ± 0.28, $P = 0.1099$; Fig. 5d).

GSK-J1 Affects Apoptosis in Developing Retina

Since we observed that GSK-J1 might cause aberrant cell proliferation, we next evaluated whether the treatment with this molecule has an influence on apoptosis during retinal development.

Twenty-four hours after GSK-J1 injection, the levels of the apoptotic cells were measured ($n = 3$ per group), and the result demonstrated a higher number of TUNEL-positive cells (0.65 ± 0.18 vs. 1.19 ± 0.26, $P = 0.0162$) in the eye injected with the blocker. Taking into account the BrdU and TUNEL results, we next evaluated whether aberrant proliferation and changes in the proportion of apoptotic cells influence the retinal thickness. However, we were not able to detect changes in the vertical length of the transverse retinal sections (139.56 ± 5.11 vs. 130.04 ± 4.53, $P = 0.210$; Fig. 6).

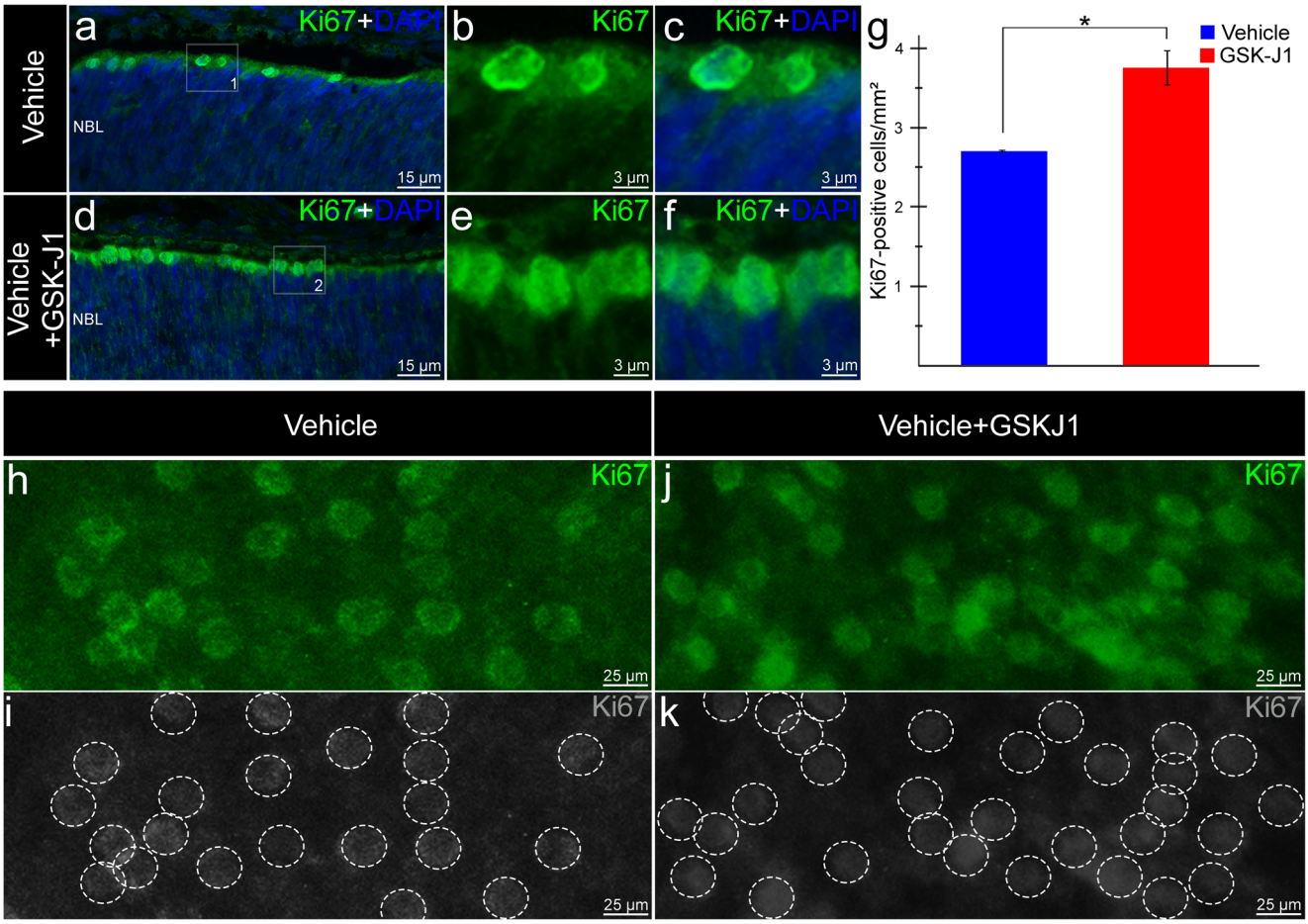

Fig. 4 Immunofluorescence analysis of Ki67 (green) in transverse sections and whole mounts of developing rat retina after GSK-J1 subretinal injection. **a** Representative immunostaining of Ki67 in transverse sections of retinas of 2-day-old rats (P2) counterstained with 4′,6-diamidino-2-phenylindole (DAPI, blue) 48 h after vehicle injection. **b**, **c** High magnification of selected area 1 showing that the Ki67-positive cells are mainly located in the outer margin of the neuroblastic layer (NBL). **d** Representative immunostaining of Ki67 in transverse sections of retinas of P2 animals counterstained with DAPI (blue) 48 h after GSK-J1 injection. **e**, **f** High magnification of selected area 2 showing numerous Ki67-positive cells located in the outer margin of the NBL. **g** The graph represents the number of Ki67-positive cells in retinas treated with vehicle versus GSK-J1. We detected significant differences on comparing vehicle and GSK-J1 groups ($P = 0.0348$, $n = 6$ per group). **h** Representative immunostaining of Ki67 in P2 retina whole mount 48 h after vehicle injection. **i** Black and white images were used to apply identification masks to better visualize the Ki67-positive cells in the whole mounts. **j** Representative immunostaining of Ki67 in P2 retina whole mount 48 h after GSK-J1 injection showing a decrease in the number of Ki67-positive cells. **k** Black and white images were used to apply identification masks to better visualize the Ki67-positive cells in the whole mounts

GSK-J1 Affects Neuronal Maturation in Developing Retina

Considering that GSK-J1 treatment increased the number of BrdU- and Ki67-positive cells, we next focused on the number of newly generated neurons/immature neurons with DCX staining. This protein has been considered a marker for newly generated immature neurons [23]. Interestingly, our data evidenced that the number of DCX-positive cells in the outer plexiform layer was significantly higher (1.48 ± 0.20 vs. 2.66 ± 0.40, $P = 0.0316$) in the retinas treated with the blocker (Fig. 7). Moreover, we also determined that the length of the filaments was longer in the retinas treated with GSK-J1 (12.03 ± 0.47 vs. 18.80 ± 0.40, $P = 0.0093$). On the other hand, we were not able to detect a significant change in the number of filaments (13.24 ± 1.50 vs. 13.83 ± 2.73, $P = 0.793$, data not shown).

GSK-J1 Affects Differentiation of Specific Neuronal Subtypes in Developing Retina

To evaluate the effects of GSK-J1 on postnatal retinal bipolar cells cytogenesis, we performed immunofluorescence experiments using anti-protein kinase C alpha (PKCα) as a marker of bipolar cells 12 days after subretinal injection. At P12, the number of PKCα-positive cells in the outer INL decreased significantly (5.21 ± 0.58 vs. 4.16 ± 0.36, $P = 0.0341$) in the retinas treated with the blocker (Fig. 8a–d, m). We next evaluated whether the differentiation of other neuronal subtypes was affected after subretinal injection of GSK-J1. To this end,

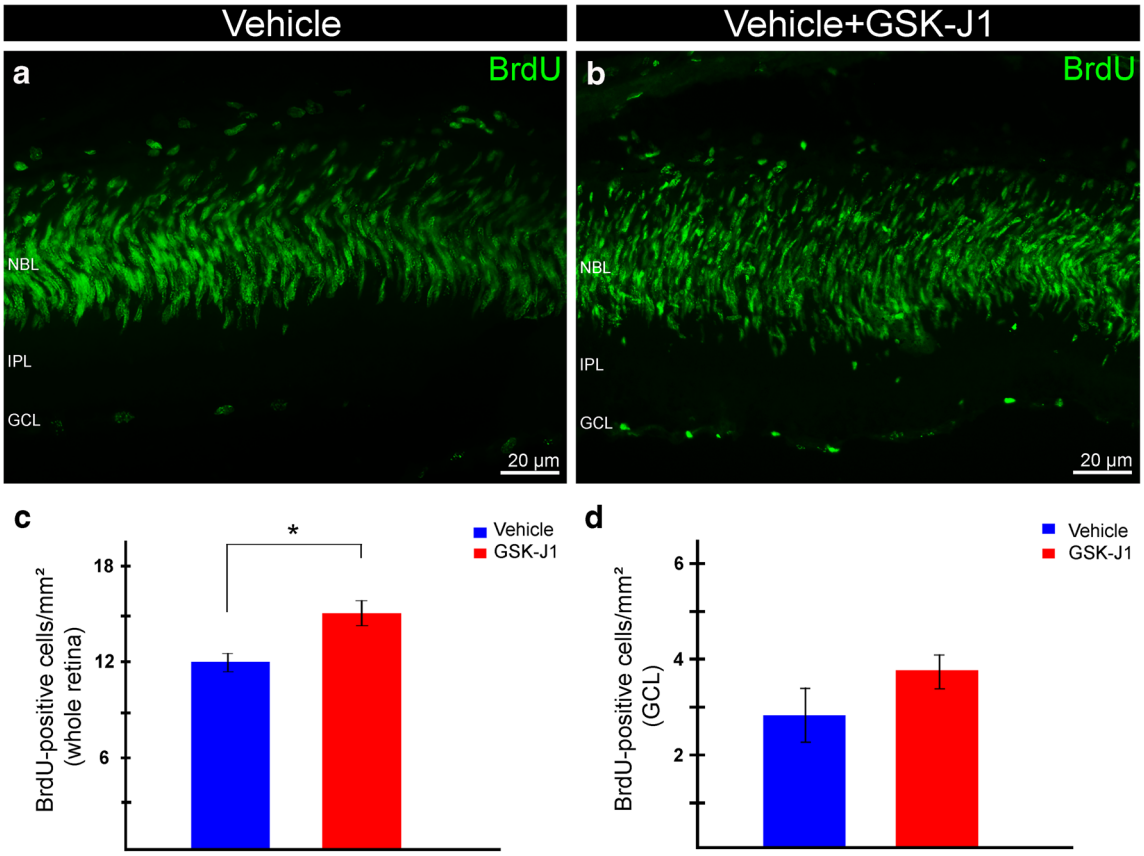

Fig. 5 Analysis of 5-bromo-2′-deoxyuridine (BrdU, green) in transverse sections of developing rat retina after GSK-J1 subretinal injection. **a** Representative staining of anti-BrdU in retinas of 2-day-old rats (P2) 48 h after vehicle injection. **b** Representative staining of anti-BrdU in P2 retinas 48 h after GSK-J1 injection. **c** The graph represents the number of BrdU-positive cells in the whole retina of the eyes injected with vehicle and GSK-J1. We were able to detect a significant increase in the number of BrdU-positive cells in the retinas treated with GSK-J1 ($P = 0.0116$, $n = 6$ per group). **d** The graph represents the number of BrdU-positive cells located in the ganglion cell layer (GCL). We were not able to detect significant changes when retinas injected with vehicle and GSK-J1 were compared ($P = 0.1099$, $n = 6$ per group)

we performed experiments using anti-parvalbumin (PV) and choline acetyltransferase (ChAT). We were not able to detect significant changes in the number of PV-positive cells in both INL (2.96 ± 0.34 vs. 2.70 ± 0.15, $P = 0.485$) (Fig. 8e–h, n) and GCL (0.43 ± 0.07 vs. 0.34 ± 0.09, $P = 0.353$). Similarly, we also were not able to detect statistically significant changes in the number of ChAT-positive cells in the INL (0.57 ± 0.04 vs. 0.58 ± 0.05, $P = 0.815$) and GCL (0.48 ± 0.03 vs. 0.46 ± 0.04, $P = 0.774$) (Fig. 8i–l, o).

Discussion

The development and application of small molecules as inhibitors of histone post-translational modifications have received attention in recent years [24, 25]. In this regard, important studies have been conducted to elucidate the role of several molecules in different cell lines and also in vivo, including GSK-J1 and ethyl ester form GSK-J4 [26–29]. On the other hand, Jmjd3 is recognized as one of the three histone demethylases that acts on H3K27 site [15]. Generally, this histone demethylase acts on histone residue, and it can also regulate demethylation of non-histone proteins such as in retinoblastoma [30–32]. In fact, Jmjd3 plays various roles in a context-dependent manner in different cell types since it is required for cell proliferation, cellular differentiation, senescence, and lineage commitment [17, 33]. Since it was previously reported that Jmjd3 has dynamic expression pattern from the embryonic stage to the adult retina [18], in the present study, we focused on the role of GSK-J1 as a blocker of JmJd3 in the early postnatal stage of rat retinal development.

In early postnatal development, JmJd3 is located mainly in differentiated neurons, but we also were able to detect the presence of this histone demethylase in undifferentiated cells. We determined that the blockade of Jmjd3 with GSK-J1 influences cell proliferation, which was evidenced by the higher rate of proliferative cells in the neuroblastic layer 48 h after the pharmacological intervention. In cancer cell lines, knockdown of *Jmjd3* can suppress the expression of cell cycle inhibitor $p^{15INK4B}$ that inhibits G1 progression [34]. Taking this into

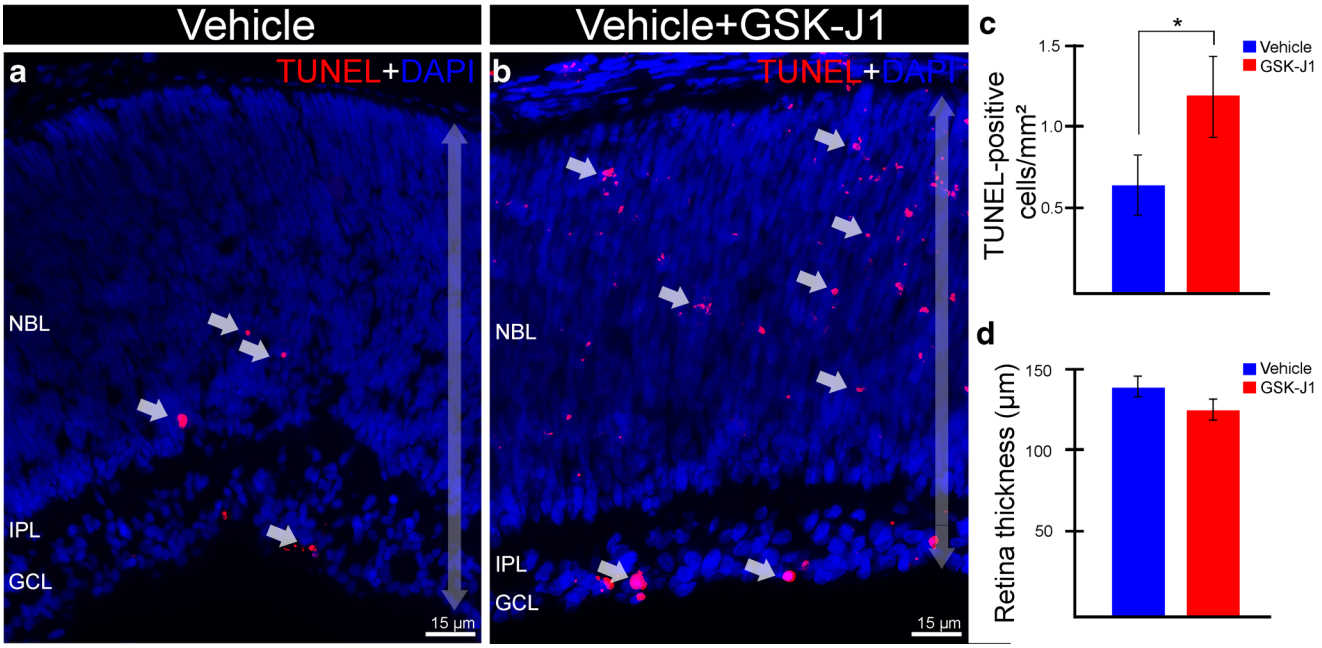

Fig. 6 Terminal deoxynucleotidyl transferase dUTP nick end labeling (TUNEL, green) analysis in transverse sections of developing rat retina counterstained with 4′,6-diamidino-2-phenylindole (DAPI, blue) after GSK-J1 subretinal injection. **a** Representative image of the retina showing TUNEL-positive cells (white arrows) 24 h after vehicle injection. The semitransparent vertical arrow represents retinal thickness. **b** Representative image of the retina showing TUNEL-positive cells (white arrows) 24 h after GSK-J1 injection. The semitransparent vertical arrow represents retinal thickness. **c** The graph represents the number of TUNEL-positive cells, which is significantly higher in the eyes injected with GSK-J1 ($P = 0.0162$, $n = 3$ per group). **d** The graph represents the mean and the standard error of the mean of the retinal thickness in eyes injected with the vehicle and GSK-J1. We were not able to detect changes when retinas treated with vehicle and GSK-J1 were compared ($P = 0.210$, $n = 3$ per group)

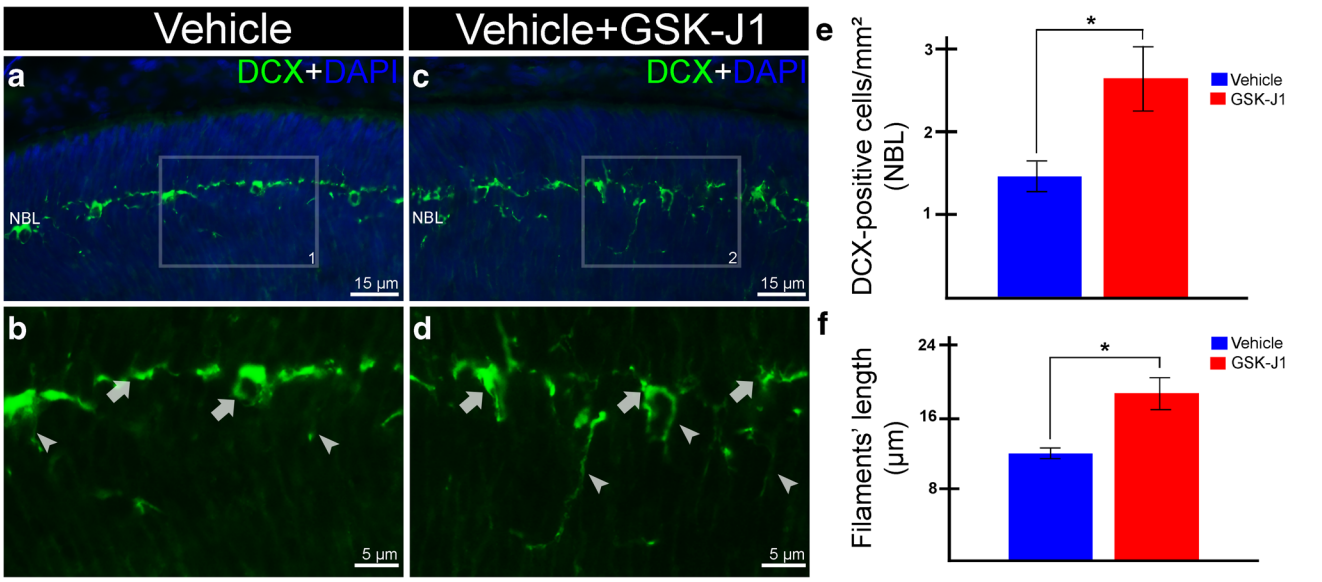

Fig. 7 Immunofluorescence analysis of microtubule-associated protein doublecortin (DCX, green) in transverse sections of developing rat retina counterstained with 4′,6-diamidino-2-phenylindole (DAPI, blue) after GSK-J1 subretinal injection. **a** Representative immunostaining of DCX in retinas of 2-day-old rats (P2) 48 h after vehicle injection. **b** High magnification of selected area 1 showing DCX-positive cells in detail. The arrows demonstrate the stained soma, whereas the arrowheads indicate the filaments. **c** Representative immunostaining of DCX in P2 retinas after GSK-J1 injection. **d** High magnification of selected area 2 showing DCX-positive cells in detail. The arrows indicate the stained soma, whereas the arrowheads demonstrate the filaments. **e** The graph represents the number of DCX-positive cells in the NBL, which is significantly higher in retinas treated with GSK-J1 ($P = 0.0316$, $n = 6$ per group). **f** The graph represents the length of filaments. We also observed that the length of the filaments increased in retinas treated with GSK-J1 ($P = 0.0093$, $n = 6$ per group)

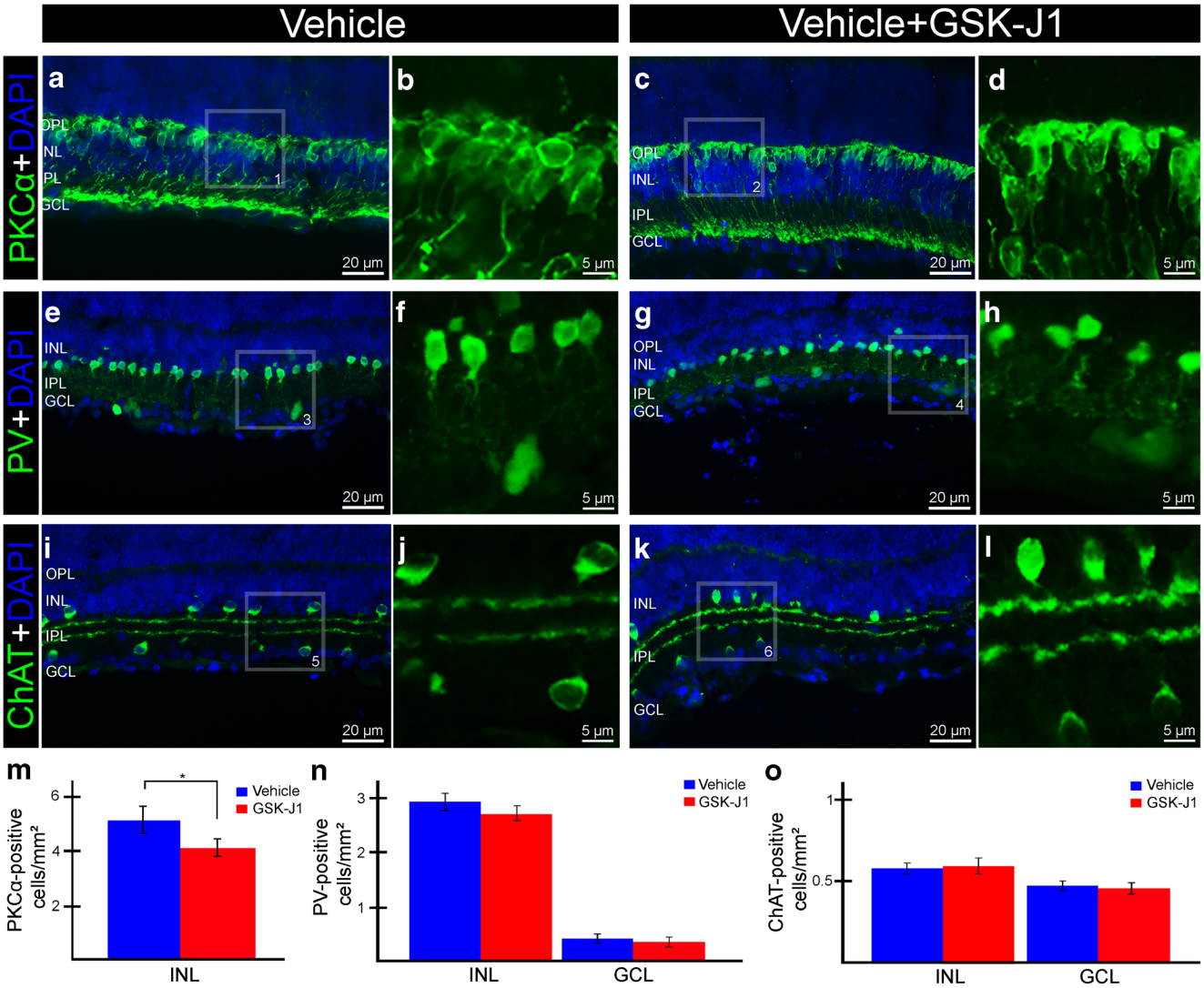

Fig. 8 Immunofluorescence analysis of specific neuronal cell markers in transverse retinal sections of 12-day-old rats (P12) counterstained with 4′,6-diamidino-2-phenylindole (DAPI, blue) 12 days after GSK-J1 subretinal injection. **a** Representative immunostaining of protein kinase C alpha (PKCα, green) in the retina after vehicle injection. **b** High magnification of selected area 1 showing numerous PKCα-positive cells, which considering the morphology and location, are presumptive rod-on bipolar cells. **c** Representative immunostaining of the PKCα-positive cells in the retina after GSK-J1 injection. **d** High magnification of selected area 2 showing the typical shape of rod-on bipolar cells. **e** Representative immunostaining of the parvalbumin (PV, green) in the retina after vehicle injection. PV-positive cells are located in both inner nuclear layer (INL) and ganglion cell layer (GCL). (F) High magnification of selected area 3 showing the typical PV-positive cells morphology, located in both INL and GCL. **g** Representative immunostaining of PV in the retina after GSK-J1 injection. **h** High magnification of selected area 4 showing PV-positive cells in detail. **i** Representative immunostaining of choline acetyltransferase (ChAT) in the retina after vehicle injection. ChAT-positive cells are located in INL and GCL. **j** High magnification of selected area 5 showing ChAT-positive cells in detail. **k** Representative immunostaining of ChAT in the retina after GSK-J1injection. **l** High magnification of selected area 6 showing ChAT-positive cells in detail. **m** The graph represents the number of PKC-positive cells in INL. We observed a significant decrease of PKC-positive cells in retinas treated with GSK-J1 ($P = 0.0341$). **n** The graph represents the number of PV-positive cells in INL and GCL. We were not able to detect changes in the number of PV-positive cells, neither in INL ($P = 0.485$) nor GCL ($P = 0.353$). **o** The graph represents the number of ChAT-positive cells in INL and GCL. We were not able to detect changes in the number of ChAT-positive cells, neither in INL ($P = 0.815$) nor GCL ($P = 0.774$)

account, it seems feasible that the blockade of Jmjd3 in the early postnatal retina downregulates the expression of $p^{15INK4B}$, which in turn may affect the cell cycle of progenitor cells. This hypothesis is supported by our study results since we detected an increased number of Ki67-positive cells in the outer neuroblastic layer.

Interestingly, previous studies documented that the knock-down of *Jmjd3* in embryonic mouse retinal explants did not change the Ki67 expression and the number of BrdU-positive cells as well [18]. It is possible that the contradictory results are due to the differences in the developmental stage when gene silencing and/or pharmacological blocking is performed.

Moreover, ganglion cells are axotomized during the preparation of retinal explants, triggering slow degeneration of these cells in vitro. These cells are important for maintaining sufficient numbers of RPCs by regulating cell proliferation through growth factors [35]. Furthermore, it is important to stress that Jmjd3 is highly accumulated in ganglion cells, as we documented in both neonate and adult retina. In spite of all these converging evidence which could explain the results obtained in the different groups, it is possible that GSK-J1 has other potential targets other than Jmjd3 that also may influence cell proliferation.

We observed that the number of TUNEL-positive cells increased 24 h after GSK-J1 subretinal injection. It has been shown that *Jmjd3* silencing can induce apoptosis in other cell types [29, 36–38]. Also, deregulation in progenitor cells proliferation may induce apoptotic cell death [39]. In fact, a higher number of TUNEL-positive cells may be related to both aberrant proliferation caused by blocking of Jmjd3 as well as the direct influence of Jmjd3 blocking on apoptosis induction.

Since we detected the presence of aberrant proliferative cells, we speculated that GSK-J1 might have an influence on newly generated neurons. During the mouse embryonic retinal development at E14.5, DCX transcripts are present in the inner NBL [40]. Our results demonstrated that the number and the length of the filaments of DCX-positive cells increased. In fact, it seems possible that Jmjd3 blocking can interfere in the neuronal maturation in retinal development. According to previous studies, Jmjd3 is important for neurogenesis in subventricular zone [16]. Also, *Jmjd3* knockdown in embryonic stem cells causes impairment in neural commitment via downregulation of the main neurogenesis markers and inducers, such as Pax6, Nestin, and Sox1 [17]. If pharmacological blocking of Jmjd3 in the early postnatal retina has the same effect on these genes, it is possible to propose that considering the impaired expression of these neurogenesis markers, more immature cells might be detectable in the retina.

Taking into account the role of Jmjd3 in neurogenesis, we aimed to elucidate the possible role of Jmjd3 blocking through GSK-J1 in retinal differentiation. The differentiation of retinal neurons follows a conserved order in the mammalian retina where successive waves of differentiation take place [41]. In P12 rats, differentiation of retinal subtypes is virtually complete, barely matching with the opening of the eyelids (around P9–P11). Our data revealed that Jmjd3 blocking decreased the number rod bipolar cells in P12 retinas with preserved morphology; yet, we were able to detect changes in the shape of DCX-positive cells, a marker of immature neurons. With regard to the differentiated neurons, the effects of GSK-J1 were restricted to bipolar cells, which are involved in the changes in the expression of genes related to differentiation of this particular neuronal subtype. In accordance, it was previously described that knockdown of Jmjd3 downregulates *Bhlhb4* and *Vsx1* in retinal explants, and both genes are important for bipolar cell differentiation [18]. It should be emphasized that compared with the previous results that induced Jmjd3 loss of function [18], the effects that we described on rod bipolar cells seems subtle. Application of GSK-J1 should block Jmjd3 activity, as previously described in other cell types [27]. The interaction of GSK-J1 and Jmjd3 was proposed based on crystallization analysis, and selectivity was demonstrated in the mass spectrometric assay. In our study, we were able to determine that the application of GSK-J1 downregulates levels of H3k27 me3. In spite of this evidence, it can be expected that direct knockdown strategies might cause more pronounced effects when compared with an indirect approach as provided by epigenetically related manipulations.

In conclusion, our data revealed that GSK-J1 influences cell proliferation, apoptosis, and differentiation of specific neuronal subtypes in developing retina. In this regard, high throughput screening would be a useful tool to decipher which specific molecular mechanisms are regulated by this small molecule in each of these processes. In spite of these considerations, it is important to stress that molecules with potential to induce epigenetic effects show promising applications in the treatment of CNS diseases. In fact, according to transcriptomic analysis, GSK-J1 has a selective inhibitory role on several immune- and inflammation-related genes in microglial cells. Therefore, GSK-J1 may have a potential influence on the treatment of neuroinflammatory diseases [42]. Furthermore, treatment based on the ethyl ester form of GSK-J4 decreased the development of experimental autoimmune encephalomyelitis (EAE) in mice [43]. Indeed, several retinal diseases such as glaucoma and diabetic retinopathy are characterized by chronic neuroinflammation [44]. In these diseases, reactive microglial cells are present in the retina [44]. In this respect, it seems interesting to decode the influence of GSK-J1 on the microglial activation and consequent impact on retinal diseases.

Acknowledgments We are grateful to Erika Reime Kinjo, Guilherme Shigueto Vilar Higa, and Vera Paschon, Neurogenetics Lab assistants, Animal Facility, at Federal University of ABC.

Funding information This research was supported by Fundação de Amparo à Pesquisa do Estado de São Paulo (FAPESP, #2013/07458-2, #2014/16711-6, #2015/04495-0, #2017/26439-0), Conselho Nacional de Desenvolvimento Científico e Tecnológico (CNPq, #431000/2016-6, #308608/2014-3), and Universidade Federal do ABC (UFABC).

Compliance with Ethical Standards

The experiments on animals were conducted considering the guidelines of the NIH and the Brazilian Society for Laboratory Animals. The experimental protocol (9965240217) was approved by the Ethics Committee of Federal University of ABC.

References

1. Seung HS, Sumbul U (2014) Neuronal cell types and connectivity: lessons from the retina. Neuron 83(6):1262–1272. https://doi.org/10.1016/j.neuron.2014.08.054
2. Bassett EA, Wallace VA (2012) Cell fate determination in the vertebrate retina. Trends Neurosci 35(9):565–573. https://doi.org/10.1016/j.tins.2012.05.004
3. Laugesen A, Helin K (2014) Chromatin repressive complexes in stem cells, development, and cancer. Cell Stem Cell 14(6):735–751. https://doi.org/10.1016/j.stem.2014.05.006
4. Aldiri I, Xu B, Wang L, Chen X, Hiler D, Griffiths L, Valentine M, Shirinifard A et al (2017) The dynamic epigenetic landscape of the retina during development, reprogramming, and tumorigenesis. Neuron 94(3):550–568 e510. https://doi.org/10.1016/j.neuron.2017.04.022
5. Seritrakul P, Gross JM (2017) Tet-mediated DNA hydroxymethylation regulates retinal neurogenesis by modulating cell-extrinsic signaling pathways. PLoS Genet 13(9):e1006987. https://doi.org/10.1371/journal.pgen.1006987
6. Bowman GD, Poirier MG (2015) Post-translational modifications of histones that influence nucleosome dynamics. Chem Rev 115(6):2274–2295. https://doi.org/10.1021/cr500350x
7. Prabakaran S, Lippens G, Steen H, Gunawardena J (2012) Post-translational modification: nature's escape from genetic imprisonment and the basis for dynamic information encoding. Wiley Interdiscip Rev Syst Biol Med 4(6):565–583. https://doi.org/10.1002/wsbm.1185
8. Bannister AJ, Kouzarides T (2011) Regulation of chromatin by histone modifications. Cell Res 21(3):381–395. https://doi.org/10.1038/cr.2011.22
9. Kooistra SM, Helin K (2012) Molecular mechanisms and potential functions of histone demethylases. Nat Rev Mol Cell Biol 13(5):297–311. https://doi.org/10.1038/nrm3327
10. Hansen KH, Bracken AP, Pasini D, Dietrich N, Gehani SS, Monrad A, Rappsilber J, Lerdrup M et al (2008) A model for transmission of the H3K27me3 epigenetic mark. Nat Cell Biol 10(11):1291–1300. https://doi.org/10.1038/ncb1787
11. Margueron R, Reinberg D (2011) The polycomb complex PRC2 and its mark in life. Nature 469(7330):343–349. https://doi.org/10.1038/nature09784
12. Iida A, Iwagawa T, Baba Y, Satoh S, Mochizuki Y, Nakauchi H, Furukawa T, Koseki H et al (2015) Roles of histone H3K27 trimethylase Ezh2 in retinal proliferation and differentiation. Dev Neurobiol 75(9):947–960. https://doi.org/10.1002/dneu.22261
13. Aldiri I, Moore KB, Hutcheson DA, Zhang J, Vetter ML (2013) Polycomb repressive complex PRC2 regulates Xenopus retina development downstream of Wnt/beta-catenin signaling. Development 140(14):2867–2878. https://doi.org/10.1242/dev.088096
14. Zhang J, Taylor RJ, La Torre A, Wilken MS, Cox KE, Reh TA, Vetter ML (2015) Ezh2 maintains retinal progenitor proliferation, transcriptional integrity, and the timing of late differentiation. Dev Biol 403(2):128–138. https://doi.org/10.1016/j.ydbio.2015.05.010
15. Swigut T, Wysocka J (2007) H3K27 demethylases, at long last. Cell 131(1):29–32. https://doi.org/10.1016/j.cell.2007.09.026
16. Park DH, Hong SJ, Salinas RD, Liu SJ, Sun SW, Sgualdino J, Testa G, Matzuk MM et al (2014) Activation of neuronal gene expression by the JMJD3 demethylase is required for postnatal and adult brain neurogenesis. Cell Rep 8(5):1290–1299. https://doi.org/10.1016/j.celrep.2014.07.060
17. Burgold T, Spreafico F, De Santa F, Totaro MG, Prosperini E, Natoli G, Testa G (2008) The histone H3 lysine 27-specific demethylase Jmjd3 is required for neural commitment. PLoS One 3(8):e3034. https://doi.org/10.1371/journal.pone.0003034
18. Iida A, Iwagawa T, Kuribayashi H, Satoh S, Mochizuki Y, Baba Y, Nakauchi H, Furukawa T et al (2014) Histone demethylase Jmjd3 is required for the development of subsets of retinal bipolar cells. Proc Natl Acad Sci U S A 111(10):3751–3756. https://doi.org/10.1073/pnas.1311480111
19. Tough DF, Tak PP, Tarakhovsky A, Prinjha RK (2016) Epigenetic drug discovery: breaking through the immune barrier. Nat Rev Drug Discov 15(12):835–853. https://doi.org/10.1038/nrd.2016.185
20. Becker S, Wang H, Stoddard GJ, Hartnett ME (2017) Effect of subretinal injection on retinal structure and function in a rat oxygen-induced retinopathy model. Mol Vis 23:832–843
21. Kihara AH, Santos TO, Paschon V, Matos RJ, Britto LR (2008) Lack of photoreceptor signaling alters the expression of specific synaptic proteins in the retina. Neuroscience 151(4):995–1005. https://doi.org/10.1016/j.neuroscience.2007.09.088
22. Dunn KW, Kamocka MM, McDonald JH (2011) A practical guide to evaluating colocalization in biological microscopy. Am J Physiol Cell Physiol 300(4):C723–C742. https://doi.org/10.1152/ajpcell.00462.2010
23. Rao MS, Shetty AK (2004) Efficacy of doublecortin as a marker to analyse the absolute number and dendritic growth of newly generated neurons in the adult dentate gyrus. Eur J Neurosci 19(2):234–246
24. Dekker FJ, van den Bosch T, Martin NI (2014) Small molecule inhibitors of histone acetyltransferases and deacetylases are potential drugs for inflammatory diseases. Drug Discov Today 19(5):654–660. https://doi.org/10.1016/j.drudis.2013.11.012
25. Mackeen MM, Kramer HB, Chang KH, Coleman ML, Hopkinson RJ, Schofield CJ, Kessler BM (2010) Small-molecule-based inhibition of histone demethylation in cells assessed by quantitative mass spectrometry. J Proteome Res 9(8):4082–4092. https://doi.org/10.1021/pr100269b
26. Heinemann B, Nielsen JM, Hudlebusch HR, Lees MJ, Larsen DV, Boesen T, Labelle M, Gerlach LO et al (2014) Inhibition of demethylases by GSK-J1/J4. Nature 514(7520):E1–E2. https://doi.org/10.1038/nature13688
27. Kruidenier L, Chung CW, Cheng Z, Liddle J, Che K, Joberty G, Bantscheff M, Bountra C et al (2012) A selective jumonji H3K27 demethylase inhibitor modulates the proinflammatory macrophage response. Nature 488(7411):404–408. https://doi.org/10.1038/nature11262
28. Bao B, He Y, Tang D, Li W, Li H (2017) Inhibition of H3K27me3 histone demethylase activity prevents the proliferative regeneration of zebrafish lateral line neuromasts. Front Mol Neurosci 10:51. https://doi.org/10.3389/fnmol.2017.00051
29. Yang D, Okamura H, Teramachi J, Haneji T (2015) Histone demethylase Utx regulates differentiation and mineralization in osteoblasts. J Cell Biochem 116(11):2628–2636. https://doi.org/10.1002/jcb.25210
30. Zhang F, Xu L, Xu L, Xu Q, Li D, Yang Y, Karsenty G, Chen CD (2015) JMJD3 promotes chondrocyte proliferation and hypertrophy during endochondral bone formation in mice. J Mol Cell Biol 7(1):23–34. https://doi.org/10.1093/jmcb/mjv003
31. Tang B, Qi G, Tang F, Yuan S, Wang Z, Liang X, Li B, Yu S et al (2016) Aberrant JMJD3 expression upregulates slug to promote migration, invasion, and stem cell-like behaviors in hepatocellular carcinoma. Cancer Res 76(22):6520–6532. https://doi.org/10.1158/0008-5472.CAN-15-3029
32. Zhao L, Zhang Y, Gao Y, Geng P, Lu Y, Liu X, Yao R, Hou P et al (2015) JMJD3 promotes SAHF formation in senescent WI38 cells by triggering an interplay between demethylation and phosphorylation of RB protein. Cell Death Differ 22(10):1630–1640. https://doi.org/10.1038/cdd.2015.6
33. Zhao W, Li Q, Ayers S, Gu Y, Shi Z, Zhu Q, Chen Y, Wang HY et al (2013) Jmjd3 inhibits reprogramming by upregulating expression

of INK4a/Arf and targeting PHF20 for ubiquitination. Cell 152(5): 1037–1050. https://doi.org/10.1016/j.cell.2013.02.006

34. Tokunaga R, Sakamoto Y, Nakagawa S, Miyake K, Izumi D, Kosumi K, Taki K, Higashi T et al (2016) The prognostic significance of histone lysine demethylase JMJD3/KDM6B in colorectal cancer. Ann Surg Oncol 23(2):678–685. https://doi.org/10.1245/s10434-015-4879-3
35. Mu X, Fu X, Sun H, Liang S, Maeda H, Frishman LJ, Klein WH (2005) Ganglion cells are required for normal progenitor—cell proliferation but not cell-fate determination or patterning in the developing mouse retina. Curr Biol 15(6):525–530. https://doi.org/10.1016/j.cub.2005.01.043
36. Sui A, Xu Y, Li Y, Hu Q, Wang Z, Zhang H, Yang J, Guo X et al (2017) The pharmacological role of histone demethylase JMJD3 inhibitor GSK-J4 on glioma cells. Oncotarget 8(40):68591–68598. https://doi.org/10.18632/oncotarget.19793
37. Zhang Y, Shen L, Stupack DG, Bai N, Xun J, Ren G, Han J, Li L et al (2016) JMJD3 promotes survival of diffuse large B-cell lymphoma subtypes via distinct mechanisms. Oncotarget 7(20):29387–29399. https://doi.org/10.18632/oncotarget.8836
38. Morozov VM, Li Y, Clowers MM, Ishov AM (2017) Inhibitor of H3K27 demethylase JMJD3/UTX GSK-J4 is a potential therapeutic option for castration resistant prostate cancer. Oncotarget 8(37): 62131–62142. https://doi.org/10.18632/oncotarget.19100
39. Dyer MA, Cepko CL (2001) Regulating proliferation during retinal development. Nat Rev Neurosci 2(5):333–342. https://doi.org/10.1038/35072555
40. Reiner O, Coquelle FM, Peter B, Levy T, Kaplan A, Sapir T, Orr I, Barkai N et al (2006) The evolving doublecortin (DCX) superfamily. BMC Genomics 7:188. https://doi.org/10.1186/1471-2164-7-188
41. Martins RA, Pearson RA (2008) Control of cell proliferation by neurotransmitters in the developing vertebrate retina. Brain Res 1192:37–60. https://doi.org/10.1016/j.brainres.2007.04.076
42. Das A, Arifuzzaman S, Yoon T, Kim SH, Chai JC, Lee YS, Jung KH, Chai YG (2017) RNA sequencing reveals resistance of TLR4 ligand-activated microglial cells to inflammation mediated by the selective jumonji H3K27 demethylase inhibitor. Sci Rep 7(1):6554. https://doi.org/10.1038/s41598-017-06914-5
43. Donas C, Carrasco M, Fritz M, Prado C, Tejon G, Osorio-Barrios F, Manriquez V, Reyes P et al (2016) The histone demethylase inhibitor GSK-J4 limits inflammation through the induction of a tolerogenic phenotype on DCs. J Autoimmun 75:105–117. https://doi.org/10.1016/j.jaut.2016.07.011
44. Madeira MH, Boia R, Santos PF, Ambrosio AF, Santiago AR (2015) Contribution of microglia-mediated neuroinflammation to retinal degenerative diseases. Mediat Inflamm 2015:673090. https://doi.org/10.1155/2015/673090